Catalysis Science & Technology

PAPER

Cite this: *Catal. Sci. Technol.*, 2015, 5, 389

Effect of preparation methods on the activity of VO_x/CeO_2 catalysts for the selective catalytic reduction of NO_x with NH_3†

Zhihua Lian, Fudong Liu and Hong He*

Received 17th July 2014,
Accepted 26th August 2014

DOI: 10.1039/c4cy00935e

www.rsc.org/catalysis

The effect of preparation methods on the activity of VO_x/CeO_2 catalysts for the selective catalytic reduction of NO_x with NH_3 was fully studied. VO_x/CeO_2 prepared by a simple homogeneous precipitation method showed higher NH_3-SCR activity and higher SO_2 and H_2O resistance than catalysts prepared by other methods. Lower CeO_2 crystallinity on the surface, better dispersion of vanadium species, and higher surface concentration of vanadium species together with more acid sites were all responsible for the higher SCR activity of VO_x/CeO_2 prepared by the homogeneous precipitation method. The NH_3-SCR reaction over VO_x/CeO_2 catalysts mainly followed the Eley–Rideal mechanism, in which gaseous NO reacted with adsorbed NH_3 species to finally form N_2 and H_2O.

1. Introduction

Nitrogen oxides (NO and NO_2), one of the major sources of air pollution, result from automobile exhaust gas and industrial combustion of fossil fuels.[1] They contribute to a variety of environmentally harmful effects such as photochemical smog, acid rain, and haze formation.[2] The selective catalytic reduction of NO_x with NH_3 (NH_3-SCR) in the presence of excess oxygen has proved to be the most efficient technology for the removal of nitrogen oxides from stationary and mobile sources.[2,3] Many catalysts have been investigated, and V_2O_5–$WO_3(MoO_3)/TiO_2$ has been widely applied as an industrial catalyst for many years due to its high catalytic activity and SO_2 resistance.[4,5] However, some problems remain for the use of V_2O_5–$WO_3(MoO_3)/TiO_2$, such as the narrow operation temperature window of 300–400 °C, low N_2 selectivity and high conversion of SO_2 to SO_3 at high temperatures.[4,6,7] In addition, the high concentration of ash containing K_2O, CaO, As_2O_3, *etc.* in the flue gas reduces the performance and longevity of V_2O_5–$WO_3(MoO_3)/TiO_2$ catalyst in this temperature range.[8,9] Therefore, a lot of studies have been performed to develop new NH_3-SCR catalyst systems or to improve vanadium-based catalysts, especially at low temperatures.[10–15]

Vanadium-based catalysts with high loading amounts usually exhibit high NH_3-SCR activity and SO_2 resistance at low temperatures.[16,17] For example, V_2O_5/AC catalysts were found to exhibit high catalytic activity in the NO–NH_3–O_2 reaction at low temperatures.[18–20] Therefore, we chose to investigate and optimize vanadium-based catalysts for practical applications. On the other hand, cerium-based catalysts have also been studied extensively due to their high oxygen storage capacity and excellent redox properties, showing high NH_3-SCR activity in the medium or high temperature ranges. In our previous study, Ce/TiO_2 catalysts have exhibited highly effective NH_3-SCR activity.[21,22] Furthermore, V_2O_5/CeO_2 catalysts have also been attracting much attention for their performance in various catalytic reactions. Gu *et al.*[23] have used V_2O_5/CeO_2 catalysts for the selective oxidation of toluene and found that the loading of V_2O_5 and the calcination temperature influenced the surface structures of dispersed vanadium species as well as the surface acidity and redox properties, which have significant effects on the catalytic activity. In the NH_3-SCR reaction, a previous study by Li *et al.*[24] showed that V_2O_5/CeO_2 catalysts exhibited high NH_3-SCR activity at low temperature, and the NO conversion increased significantly with increasing V_2O_5 loading. It was reported that the $V_{0.75}Ce$ oxide catalyst exhibited higher NH_3-SCR activity than the conventional V_2O_5–WO_3/TiO_2 catalyst below 350 °C.[25] Although V/Ce oxide catalysts have shown great catalytic activity, their properties are not well understood and should be investigated in more detail. It is also necessary to decrease the vanadium content due to its toxicity.

In many cases, the activity of catalysts is highly dependent on the preparation method. Therefore, in this study we

State Key Joint Laboratory of Environment Simulation and Pollution Control, Research Center for Eco-Environmental Sciences, Chinese Academy of Sciences, 18 Shuangqing Road, Haidian District, Beijing 100085, China.
E-mail: honghe@rcees.ac.cn; Fax: +86 10 62849123; Tel: +86 10 62849123

† Electronic supplementary information (ESI) available: NO_x conversion over VO_x/CeO_2 with different loadings; the N_2 selectivity in NH_3-SCR reaction; NH_3-SCR activity after SO_2 poisoning; NH_3/NO conversion in separate NH_3 or NO oxidation reactions; and the band intensity of nitrate species calculated from DRIFTS of VO_x/CeO_2 catalysts. See DOI: 10.1039/c4cy00935e

systematically investigated VO_x/CeO_2 catalysts in depth, especially the effects of preparation methods on the catalyst structure and activity in NH_3-SCR of NO_x. Even with low loading content of vanadia, the catalysts could still exhibit excellent catalytic performance for the $DeNO_x$ process. In addition, the VO_x/CeO_2 catalyst prepared by a simple homogeneous precipitation method (VO_x/CeO_2(P)) showed higher NH_3-SCR activity and better SO_2 resistance than catalysts prepared by other methods, mainly due to lower CeO_2 crystallinity on the surface, better dispersion of vanadium species, and higher surface concentration of vanadium species together with more acid sites.

2. Experiments

2.1 Catalyst synthesis and activity tests

The 3 wt.% VO_x/CeO_2 catalysts were prepared by four methods: the homogeneous precipitation method, rotary evaporation impregnation, incipient wetness impregnation and the sol–gel method. All of the materials were purchased from Sinopharm Chemical Reagent Co., Ltd (China) and were analytically pure, except the CeO_2 supports which were prepared by the homogeneous precipitation method, as described below.

Rotary evaporation impregnation. VO_x/CeO_2 was prepared by rotary evaporation impregnation method using CeO_2 and an aqueous solution of NH_4VO_3 ($H_2C_2O_4$ was added to facilitate the dissolution of NH_4VO_3). After impregnation, the excess water was removed using a rotary evaporator at 60 °C. The sample was first dried at 100 °C overnight followed by calcination at 500 °C in air for 3 h. The catalyst was denoted as VO_x/CeO_2(V).

Homogeneous precipitation method. Aqueous solutions of $Ce(NO_3)_3$ and NH_4VO_3 were mixed at the required mass ratio (the mass ratio of vanadium oxide was controlled at 3 wt.%). Excess urea in the aqueous solution was then added to the mixed solution. The solution was heated to 90 °C and maintained for 12 h under vigorous stirring. After filtration and washing with deionized water, the resulting precipitate was dried at 100 °C overnight and subsequently calcined at 500 °C for 3 h in air. The VO_x/CeO_2 sample prepared by the homogeneous precipitation method was denoted as VO_x/CeO_2(P).

Incipient wetness impregnation method. VO_x was deposited on CeO_2 by conventional pore volume impregnation with an aqueous solution of NH_4VO_3 in oxalic acid. After ultrasonic processing for 1 h, the material was dried at 100 °C overnight and calcined at 500 °C for 3 h. The VO_x/CeO_2 sample prepared by the incipient wetness impregnation method was denoted as VO_x/CeO_2(I).

Sol–gel method. $Ce(NO_3)_3$, NH_4VO_3 (at a ratio to yield 3 wt.% vanadium oxide) and excess citric acid were mixed in aqueous solution. The resulting mixture was stirred at room temperature for 1 h. The solution was dried at 120 °C for 12 h, resulting in a porous, foam-like solid. The foam-like precursor was calcined at 500 °C for 3 h in air in a temperature-programmed muffle furnace. The VO_x/CeO_2 sample prepared by the sol–gel method was denoted as VO_x/CeO_2(S).

Before NH_3-SCR activity testing, the catalysts were pressed, crushed and sieved to 40–60 mesh. The SCR activity tests were performed in a fixed-bed quartz flow reactor at atmospheric pressure. The reaction conditions were controlled as follows: 500 ppm NO, 500 ppm NH_3, 5 vol.% O_2, 5 vol.% H_2O (when used), 100 ppm SO_2 (when used), N_2 balance. Under ambient conditions, the total flow rate was 500 ml min^{-1} and the gas hourly space velocity (GHSV) was 50 000 h^{-1}. The effluent gas including NO, NH_3, NO_2 and N_2O was continuously analyzed with an FTIR spectrometer (Nicolet Nexus 670) equipped with a heated, low-volume multiple-path gas cell (2 m). FTIR spectra were collected after the SCR reaction reached a steady state, and the NO_x conversion and N_2 selectivity were calculated as follows:

$$\mathrm{NO}_x\ \text{conversion} = \left(1 - \frac{[\mathrm{NO}]_{\mathrm{out}} + [\mathrm{NO_2}]_{\mathrm{out}}}{[\mathrm{NO}]_{\mathrm{in}} + [\mathrm{NO_2}]_{\mathrm{in}}}\right) \times 100\%$$

$$\mathrm{N_2}\ \text{selectivity} = \frac{[\mathrm{NO}]_{\mathrm{in}} + [\mathrm{NH_3}]_{\mathrm{in}} - [\mathrm{NO_2}]_{\mathrm{out}} - 2[\mathrm{N_2O}]_{\mathrm{out}}}{[\mathrm{NO}]_{\mathrm{in}} + [\mathrm{NH_3}]_{\mathrm{in}}} \times 100\%$$

2.2 Characterization of catalysts

The surface area and pore characterization of the catalysts were obtained from N_2 adsorption/desorption analysis at −196 °C using a Quantachrome Quadrasorb SI-MP. Prior to N_2 physisorption, the catalysts were degassed at 300 °C for 5 h. Surface areas were determined by the BET equation in the 0.05–0.35 partial pressure range. Pore volumes and average pore diameters were determined by the Barrett–Joyner–Halenda (BJH) method from the desorption branches of the isotherms.

Powder X-ray diffraction measurements of the catalysts were performed using a computerized PANalytical X'Pert Pro diffractometer with Cu Kα (λ = 0.15406 nm) radiation. The data of 2θ from 10 to 80° were collected at 8° min^{-1} with a step size of 0.07°.

Visible Raman spectra of the VO_x/CeO_2 catalysts were collected at room temperature using a Spex 1877 D Triplemate spectrometer with a spectral resolution of 2 cm^{-1}. A 532 nm diode-pump solid semiconductor (DPSS) laser was used as the excitation source and the power output was about 40 mW. Before measurements, the catalysts were ground well and mounted on a spinning holder to avoid thermal damage during scanning. Raman signals were collected with conventional 90° geometry and the time for recording each spectrum was 1000 ms. The Raman spectra used in this paper were original and unsmoothed.

The H_2-TPR experiments were performed with a Micromeritics AutoChem 2920 chemisorption analyzer. The samples (50 mg) were pretreated at 300 °C under a flow of

20 vol.% O_2/Ar (50 ml min^{-1}) for 0.5 h in a quartz reactor and cooled down to room temperature (30 °C) followed by Ar purging for 0.5 h. A 50 ml min^{-1} gas flow of 10% H_2 in Ar was then passed over the samples through a cold trap to the detector. The reduction temperature was raised at 10 °C min^{-1} from 30 to 1000 °C.

X-ray photoelectron spectroscopy (XPS) spectra of the catalysts were recorded with a scanning X-ray microprobe (AXIS Ultra, Kratos Analytical Ltd.) using Al Kα radiation (1486.7 eV). All of the binding energies were calibrated using the C 1s peak (BE = 284.8 eV) as the standard.

2.3 NH_3-TPD studies

NH_3-TPD experiments were performed using a quadrupole mass spectrometer (HPR-20, Hiden Analytical Ltd.) to record the signal of NH_3 (m/z = 15 for NH). Prior to TPD experiments, the samples (100 mg) were pretreated at 400 °C under a flow of 20 vol.% O_2/Ar (50 ml min^{-1}) for 0.5 h and cooled down to room temperature (30 °C). The samples were then exposed to a flow of 2500 ppm NH_3/Ar (50 ml min^{-1}) at 30 °C for 1 h, followed by Ar purging for another 1 h. Finally, the temperature was raised to 600 °C under Ar flow at a rate of 10 °C min^{-1}.

2.4 *In situ* DRIFTS studies

In situ DRIFTS experiments were performed using an FTIR spectrometer (Nicolet Nexus 670) equipped with a smart collector and an MCT/A detector cooled by liquid nitrogen. The reaction temperature was controlled precisely by an Omega programmable temperature controller. Prior to each experiment, the sample was pretreated at 400 °C for 0.5 h under a flow of 20 vol.% O_2/N_2 and then cooled to 200 °C. The background spectra were collected under flowing N_2 and automatically subtracted from the sample spectrum. The reaction conditions were controlled as follows: 300 ml min^{-1} total flow rate, 500 ppm NH_3 or/and 500 ppm NO + 5 vol.% O_2, and N_2 balance. All spectra were recorded by accumulating 100 scans with a resolution of 4 cm^{-1}.

3. Results

3.1 Catalytic performance

3.1.1 SCR activity over VO_x/CeO_2 catalysts. The NH_3-SCR activity over VO_x/CeO_2 with different loadings is shown in Fig. S1.† 3 wt.% VO_x/CeO_2 showed much higher catalytic activity than 1%, 0.5%, and 0.1% catalysts, especially at 150–300 °C. Due to the toxicity of vanadium to the human body, a vanadium-based catalyst with very high loading was not preferred. Therefore, we chose the 3% VO_x/CeO_2 catalyst to investigate rather than catalysts with higher loading.

The NO_x conversion over VO_x/CeO_2 catalysts prepared by different methods is shown in Fig. 1. It is obvious that the preparation methods affected the catalytic activity, especially in the relatively low temperature range. VO_x/CeO_2 prepared by the simple homogeneous precipitation method exhibited the best catalytic activity, with nearly 100% NO_x conversion and 100% N_2 selectivity at temperatures above 200 °C. VO_x/CeO_2 catalysts prepared by rotary evaporation impregnation and incipient wetness impregnation method showed lower NO_x conversion than that prepared by the homogeneous precipitation method, and the catalyst prepared by the sol–gel method showed the lowest catalytic activity. All of the catalysts presented higher than 90% N_2 selectivity and only a small amount of N_2O was produced at the temperature that we investigated (as shown in Fig. S2†). The preparation methods could affect the structural properties, redox ability and surface acidity of the catalysts, resulting in different catalytic activities, which will be discussed later in this paper.

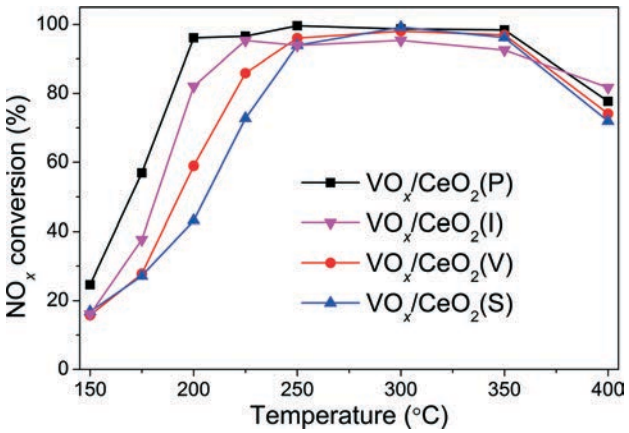

Fig. 1 NH_3-SCR activity over VO_x/CeO_2 catalysts prepared by different methods. Reaction conditions: [NO] = [NH_3] = 500 ppm, [O_2] = 5 vol.%, N_2 balance, total flow rate 500 ml min^{-1} and GHSV = 50 000 h^{-1}.

3.1.2 The influence of H_2O and SO_2 on the SCR activity of VO_x/CeO_2. The NO_x conversion over VO_x/CeO_2 catalysts in the NH_3-SCR reaction with 5 vol.% H_2O is shown in Fig. 2. Compared to NH_3-SCR activity without H_2O, NO_x conversion

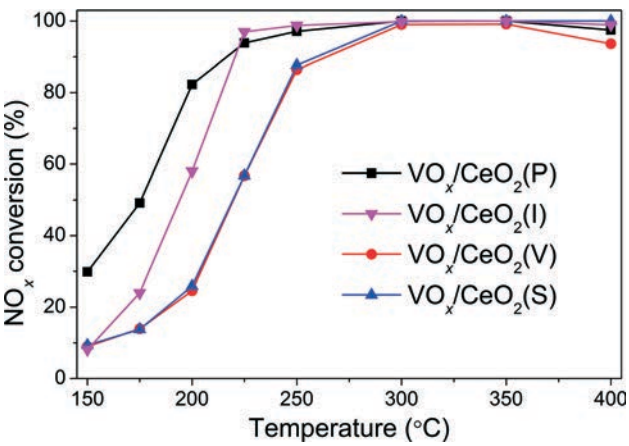

Fig. 2 NO_x conversion over VO_x/CeO_2 catalysts in NH_3-SCR reaction in the presence of H_2O. Reaction conditions: [NO] = [NH_3] = 500 ppm, [H_2O] = 5 vol.%, [O_2] = 5 vol.%, N_2 balance, total flow rate 500 ml min^{-1} and GHSV = 50 000 h^{-1}.

in the presence of H_2O over the four catalysts at low temperatures decreased in all cases to some degree, while catalytic activity at 400 °C increased from 80% to 100%. The NO_x conversion over the VO_x/CeO_2(P) catalyst at 200 °C was 80%, and only 20% NO_x conversion was obtained over VO_x/CeO_2(S) and VO_x/CeO_2(V). The VO_x/CeO_2(P) catalyst still exhibited the best catalytic performance in the presence of H_2O.

Fig. 3 shows the effect of SO_2 on the catalytic activity over VO_x/CeO_2 catalysts at 250 °C. When 100 ppm SO_2 was introduced to the gas inlet, the NO_x conversion over VO_x/CeO_2(S) decreased rapidly to as low as 60% in 24 h and could not recover to the initial activity after the removal of SO_2. The NO_x conversion over VO_x/CeO_2(V) and VO_x/CeO_2(I) catalysts also decreased, and after the introduction of SO_2, the catalytic activity recovered to some extent. However, the SO_2 poisoning behaviour over VO_x/CeO_2(P) was quite different. The NO_x conversion decreased slowly, and 93% NO_x conversion was obtained in the presence of 100 ppm SO_2 for a 24 h test. VO_x/CeO_2(P) exhibited the highest catalytic activity and the strongest resistance to SO_2. The NH_3-SCR performance of VO_x/CeO_2 catalysts after SO_2 poisoning for 24 h is shown in Fig. S3.† The activity over VO_x/CeO_2(P) was still higher than those over the other catalysts. 100% NO_x conversion could be obtained over the VO_x/CeO_2(P) catalyst at 250 °C and 70% over VO_x/CeO_2(S). This proved again that the VO_x/CeO_2(P) catalyst showed the strongest SO_2 resistance.

3.2 Catalyst characterization

3.2.1 N_2 physisorption. The surface areas and pore diameters of VO_x/CeO_2 catalysts are shown in Table 1. The VO_x/CeO_2(P) catalyst exhibited a slightly larger BET surface area and a smaller average pore diameter than VO_x/CeO_2(S), which could offer more active sites for reaction and thus be beneficial to NH_3-SCR activity. The slight difference in the specific surface area indicates that the textural structure is not the crucial factor affecting the catalytic performance.

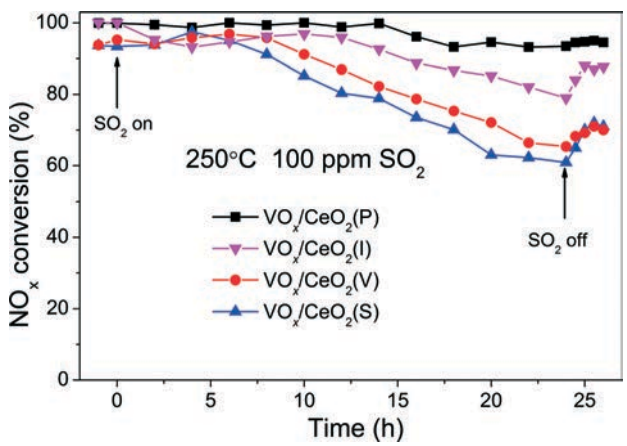

Fig. 3 Effect of SO_2 on the NH_3-SCR activity over VO_x/CeO_2 catalysts at 250 °C. Reaction conditions: [NO] = [NH_3] = 500 ppm, [SO_2] = 100 ppm, [O_2] = 5 vol.%, N_2 balance, total flow rate 500 ml min^{-1} and GHSV = 50 000 h^{-1}.

Table 1 Surface atomic concentration, BET surface areas and pore diameters of VO_x/CeO_2 catalysts

Catalysts	Surface atomic concentration[a] (%)			V/Ce atomic ratio	BET surface area (m^2 g^{-1})	Pore diameter (nm)
	Ce	V	O			
VO_x/CeO_2(P)	33.5	2.4	64.1	0.072	91.9	5.2
VO_x/CeO_2(S)	33.2	1.6	65.2	0.047	88.5	10.5

[a] According to XPS analysis.

3.2.2 XRD. The XRD patterns of VO_x/CeO_2 catalysts are shown in Fig. 4. For both catalysts, the only crystalline phase observed was CeO_2 (43-1002). No vanadium species such as V_2O_5 and $CeVO_4$ were detected, suggesting that V species were highly dispersed on the catalysts. The intensity of the CeO_2 diffraction peaks of the VO_x/CeO_2(P) catalyst was stronger than that of VO_x/CeO_2(S), indicating that the crystallinity of the CeO_2 phase of VO_x/CeO_2(P) was higher than that of VO_x/CeO_2(S).

3.2.3 Raman and XPS. The surface-sensitive techniques Raman and XPS were employed for characterization of the VO_x/CeO_2 catalysts. Fig. 5 shows the Raman results for VO_x/CeO_2(P) and VO_x/CeO_2(S) catalysts. In accordance with previous studies,[22,26] the Raman shift at 453 cm^{-1} was attributed to CeO_2 (F_{2g} mode). No evidence of vanadium-containing phases, such as V_2O_5 and $CeVO_4$, was detected for either catalyst. The CeO_2 peak intensity for the VO_x/CeO_2(P) catalyst was weaker than that for VO_x/CeO_2(S), indicating that the CeO_2 crystallinity on the surface of the VO_x/CeO_2(P) catalyst was weaker. Active sites could thus be better dispersed on the surface of VO_x/CeO_2(P).

Table 1 also shows the surface atomic concentrations of VO_x/CeO_2 catalysts derived from XPS results. VO_x/CeO_2(P) and VO_x/CeO_2(S) catalysts exhibited similar surface Ce and O concentrations. The surface V concentration of the VO_x/CeO_2(P) catalyst was 2.4%, which is much higher than that of

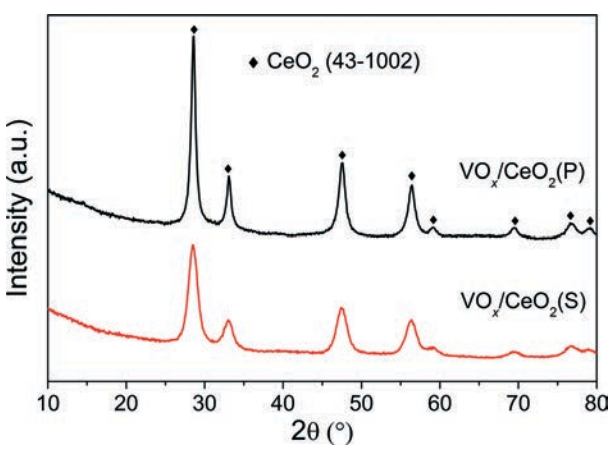

Fig. 4 XRD patterns of VO_x/CeO_2 catalysts.

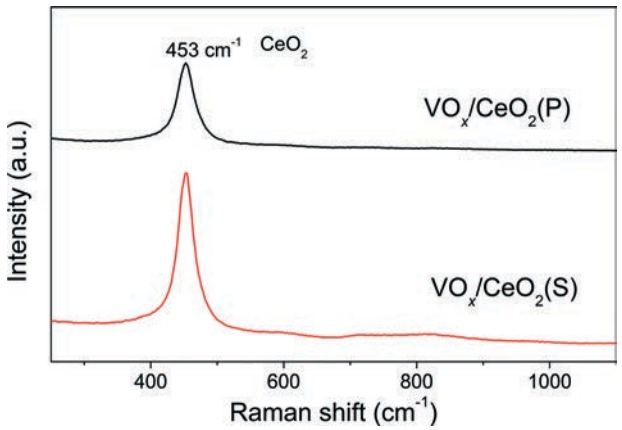

Fig. 5 Raman results of VO_x/CeO_2 catalysts.

VO_x/CeO_2(S) (1.6%). The V/Ce atomic ratio was 0.072 and 0.047 for VO_x/CeO_2(P) and VO_x/CeO_2(S), respectively. The higher surface concentration of vanadium species could result in better SCR activity.

3.2.4 H_2-TPR. H_2-TPR is frequently used to investigate the redox properties of metal oxide catalysts. Fig. 6 presents the TPR results of VO_x/CeO_2(P) and VO_x/CeO_2(S) catalysts. According to the literature,[27,28] the TPR peak around 480 °C could be attributed to the reduction of surface Ce^{4+} to Ce^{3+}. The reduction peak of well-dispersed V^{5+} species could occur at 460 °C.[29,30] The reduction peak of the CeO_2 catalyst at 471 °C could be ascribed to the reduction of surface Ce^{4+} and the peak at 760 °C could be attributed to the reduction of bulk CeO_2. Over the VO_x/CeO_2(P) and VO_x/CeO_2(S) catalysts, the reduction peaks at low temperature showed a much higher intensity than those of the CeO_2 sample mainly due to the interaction between vanadium and cerium oxides. The H_2 reduction temperature of the VO_x/CeO_2(P) catalyst was lower than that of VO_x/CeO_2(S) in the low temperature region, and the amount of H_2 consumption of the former was larger than that of the latter. In addition, NO/NH_3 oxidation activity over VO_x/CeO_2(P) was higher than that over VO_x/CeO_2(S) (as shown in Fig. S4†). This indicates that the redox capability of the VO_x/CeO_2(P) catalyst was a little greater than that of VO_x/CeO_2(S), which could contribute to the NH_3-SCR activity to some degree.

3.3 NH_3-TPD

Fig. 7 shows NH_3-TPD results over VO_x/CeO_2 catalysts using the fragment of m/z = 15 (NH) to identify NH_3. There were three NH_3 desorption peaks around 90, 250 and 470 °C on both catalysts. The desorption peaks at 90 °C were ascribed to the desorption of physisorbed NH_3. The broad desorption peaks between 150 °C and 400 °C were assigned to weak and moderate acid sites on the catalyst surface. With increasing temperature, small peaks between 400 °C and 600 °C occurred in the NH_3-TPD profiles, which are related to NH_3 molecules adsorbed on the strong acid sites of the catalysts.[31] Although the desorption temperature of VO_x/CeO_2(P) was a litter higher than that of the VO_x/CeO_2(S) catalyst, the amount of NH_3 desorption from the former was notably larger than that from the latter. This indicates that there are more acid sites on the VO_x/CeO_2(P) catalyst.

3.4 *In situ* DRIFTS

3.4.1 NH_3 adsorption. The *in situ* DRIFT spectra of NH_3 adsorption on VO_x/CeO_2(P) and VO_x/CeO_2(S) catalysts at 200 °C are shown in Fig. 8(A). After NH_3 adsorption and N_2 purging, both catalysts were covered with various NH_3 species. The bands at 1425 cm^{-1} were assigned to ionic NH_4^+ bound to the Brønsted acid sites and the bands at 1594 and 1158 cm^{-1} were attributed to coordinated NH_3 bound to the Lewis acid sites.[32,33] The bands at 1260 cm^{-1} were assigned to the amide species (–NH_2).[33] The VO_x/CeO_2(P) catalyst exhibited more acid sites than VO_x/CeO_2(S), including Brønsted acid sites and Lewis acid sites, which was in good agreement with the NH_3-TPD results.

3.4.2 NO_x adsorption. Fig. 8(B) shows the DRIFT spectra of NO + O_2 adsorption on VO_x/CeO_2(P) and VO_x/CeO_2(S) catalysts at 200 °C. When the VO_x/CeO_2 catalyst was exposed

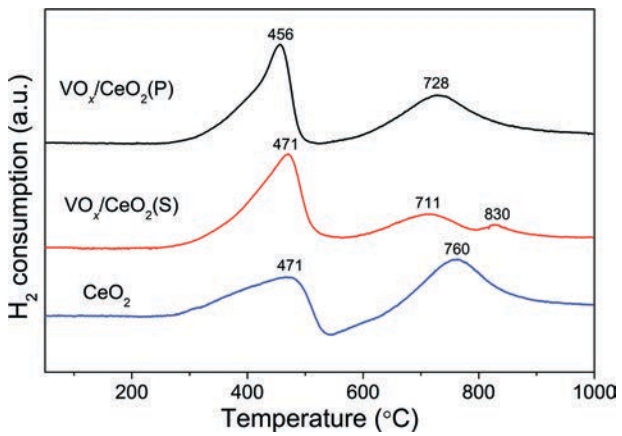

Fig. 6 H_2-TPR results over VO_x/CeO_2 catalysts.

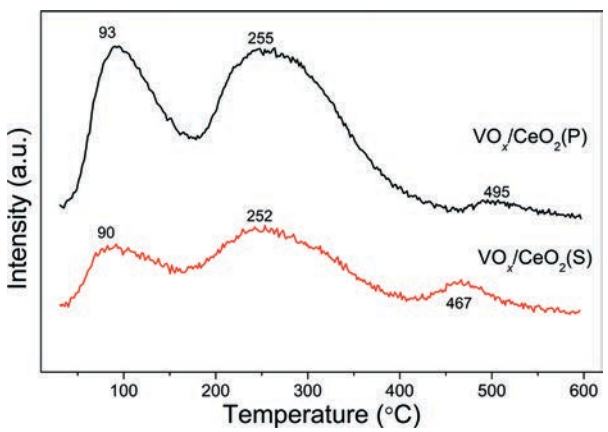

Fig. 7 NH_3-TPD results of VO_x/CeO_2 catalysts.

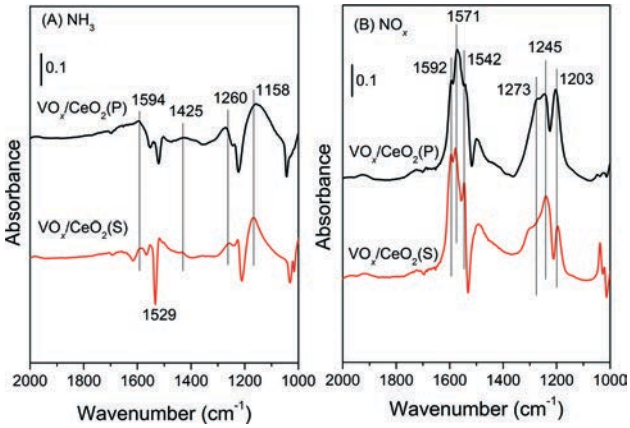

Fig. 8 DRIFT spectra of 500 ppm NH_3 adsorption (A) and 500 ppm NO + 5 vol.% O_2 adsorption (B) on VO_x/CeO_2(P) and VO_x/CeO_2(S) catalysts.

to NO + O_2, several bands assigned to nitrate species were observed. The bands at 1203 and 1592 cm^{-1} could be assigned to bridging nitrate.[34,35] The bands at 1571 and 1245 cm^{-1} were ascribed to bidentate nitrate,[32,35,36] while the bands at 1502–1542 and 1273 cm^{-1} were attributed to monodentate nitrate.[32,34] The adsorption amount of NO_x was larger on the VO_x/CeO_2(P) catalyst than that on VO_x/CeO_2(S), especially the amount of monodentate nitrate at 1273 cm^{-1}.

3.4.3 *In situ* DRIFTS of the reaction between NO + O_2 species and pre-adsorbed NH_3 species. Fig. 9(A) shows the *in situ* DRIFT spectra of the reaction between NO + O_2 species and pre-adsorbed NH_3 species on VO_x/CeO_2(P). After NH_3 pre-adsorption and N_2 purging, the VO_x/CeO_2(P) catalyst surface was covered with various NH_3 species. When NO + O_2 was introduced, the intensity of the bands attributed to NH_3 species decreased quickly and disappeared after 5 min. At the same time, bands assigned to nitrate species (monodentate nitrate at 1542, 1273 cm^{-1}, bridging nitrate at 1203, 1597 cm^{-1} and bidentate nitrate at 1571, 1245 cm^{-1}) appeared. This result suggested that the adsorbed NH_3 species, including ionic NH_4^+ and coordinated NH_3, could both react with NO_x and participate in the NH_3-SCR reactions.

For the VO_x/CeO_2(S) catalyst (Fig. 9(B)), similar bands due to NH_3 adsorption were observed after NH_3 pre-adsorption and N_2 purging. After the introduction of NO + O_2, the adsorbed NH_3 species decreased in intensity and totally vanished after 10 min, followed by the appearance of nitrate species. The adsorbed NH_3 species on VO_x/CeO_2(S) could also participate in the SCR reaction, similar to VO_x/CeO_2(P).

3.4.4 *In situ* DRIFTS of the reaction between NH_3 species and pre-adsorbed NO_x species. The catalysts were first treated with NO + O_2 for 30 min, followed by N_2 purging. When NH_3 was introduced, the IR spectra were recorded as a function of time. For the VO_x/CeO_2(P) catalyst (Fig. 10(A)), after NO + O_2 pre-adsorption and N_2 purging, the catalyst surface was covered with various nitrate species. When NH_3 was introduced, the intensity of the bands attributed to monodentate nitrate and bridging nitrate species decreased slightly. The amount of bidentate nitrate species increased markedly, which may be due to the transformation of monodentate and bridging nitrate to bidentate nitrate. The changes in band intensities of nitrate species on NO_x pre-adsorbed catalysts during the introduction of NH_3 are shown in Fig. S5.† The bands at 1425 and 1158 cm^{-1} attributed to adsorbed NH_3 species appeared after NH_3 was introduced. The adsorbed nitrate species could not easily react with adsorbed NH_3. This suggests that the adsorbed nitrate species were mostly inactive in the NH_3-SCR reaction.

For the VO_x/CeO_2(S) catalyst (Fig. 10(B)), similar bands ascribed to nitrate species were observed after NO + O_2 adsorption and N_2 purging. When NH_3 was introduced, the intensity of bridging nitrate decreased slowly and the bands attributed to monodentate and bidentate nitrate species remained unchanged. Adsorbed NH_3 species began to form on the VO_x/CeO_2(S) catalyst surface after 2 min upon NH_3

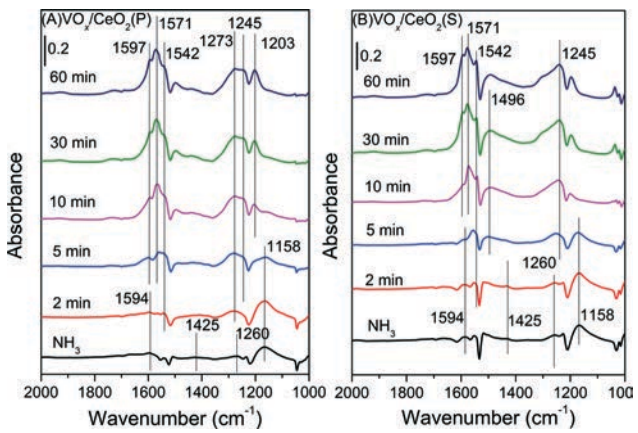

Fig. 9 *In situ* DRIFT spectra of VO_x/CeO_2(P) (A) and VO_x/CeO_2(S) (B) pretreated by exposure to 500 ppm NH_3 followed by exposure to 500 ppm NO + 5 vol.% O_2 at 200 °C.

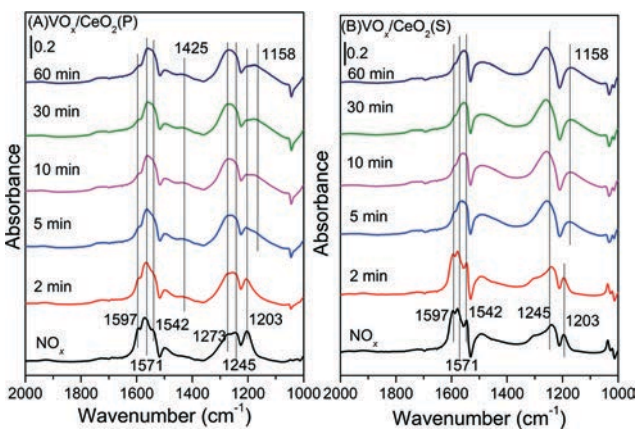

Fig. 10 *In situ* DRIFT spectra of VO_x/CeO_2(P) (A) and VO_x/CeO_2(S) (B) pretreated by exposure to 500 ppm NO + 5 vol.% O_2 followed by exposure to 500 ppm NH_3 at 200 °C.

introduction. The adsorbed nitrate could not easily take part in the NH_3-SCR reaction.

4. Discussion

4.1 The effect of preparation methods on catalytic activity

The effect of preparation methods on the catalytic activity of VO_x/CeO_2 catalysts was investigated in detail in this study. VO_x/CeO_2 prepared by the homogeneous precipitation method showed the highest SCR activity, and nearly 100% NO_x conversion plus 100% N_2 selectivity was obtained above 200 °C. In addition, VO_x/CeO_2(P) exhibited the strongest resistance to H_2O and SO_2 in NH_3-SCR.

Based on the XRD results, the crystallinity of the CeO_2 phase in the VO_x/CeO_2(P) catalyst was higher than that in VO_x/CeO_2(S). However, the Raman spectra showed that the homogeneous precipitation method restrained the crystallization of CeO_2 on the surface layer of the VO_x/CeO_2(P) catalyst. The lower surface crystallinity signifies more defects on the catalyst surface and better dispersion of vanadium species, which could enhance catalytic activity. Higher surface vanadium concentration on the VO_x/CeO_2(P) catalyst, as shown by XPS results, indicated more active sites and improved the NH_3-SCR performance.

In addition, the surface acidity of a catalyst plays an important role in the NH_3-SCR reaction. VO_x/CeO_2(P) and VO_x/CeO_2(S) showed similar specific surface areas, but the NH_3 desorption amount from the former was much larger, indicating that the VO_x/CeO_2(P) catalyst could provide more acid sites. This could result from the higher surface concentration of vanadium species, since acid sites are more prevalent on vanadium oxide than on cerium oxide. More acid sites on the VO_x/CeO_2(P) catalyst could facilitate the adsorption and activation of NH_3 during the catalytic reaction and thus enhance its catalytic activity in NH_3-SCR.

Furthermore, according to the literature,[37,38] vanadium oxide shows excellent SO_2 resistance in NH_3-SCR. Therefore, a higher surface concentration of vanadium species on the catalyst surface could enhance SO_2 resistance. The VO_x/CeO_2(P) catalyst showed higher catalytic activity in the presence of 100 ppm SO_2 than VO_x/CeO_2(S).

4.2 SCR reaction mechanism

NH_3 could adsorb on VO_x/CeO_2(P) and VO_x/CeO_2(S) catalysts to form NH_4^+ and coordinated NH_3. When NO_x was introduced, NH_3 adsorbed species disappeared quickly. Both NH_4^+ and coordinated NH_3 could react with NO_x. Monodentate, bridging and bidentate nitrates were deposited on the catalyst surface when NO + O_2 were introduced. Adsorbed nitrate species were mostly inactive in the NH_3-SCR reaction. After NH_3 was introduced, the number of monodentate and bridging nitrates reduced slightly, but the amount of bidentate nitrate increased. Gaseous NO mainly interacted with adsorbed NH_3 species on VO_x/CeO_2 catalysts to form an activated intermediate and subsequently decomposed to N_2 and H_2O according to the Eley–Rideal mechanism.[39]

5. Conclusions

VO_x/CeO_2 catalysts exhibited excellent NH_3-SCR performance. VO_x/CeO_2 prepared by a simple homogeneous precipitation method showed higher catalytic activity and better H_2O and SO_2 resistance than catalysts prepared by other methods. As high as 93% NO_x conversion was obtained in the presence of 100 ppm SO_2 for a 24 h test over the VO_x/CeO_2(P) catalyst.

The weaker crystallinity of CeO_2 in the surface layers of VO_x/CeO_2(P) implied more defects on its surface and better dispersion of vanadium species than that on VO_x/CeO_2(S). The higher surface vanadium concentration led to more acid sites on VO_x/CeO_2(P), which can absorb and activate more NH_3 species. All of these factors contributed to the higher SCR activity and SO_2 resistance of VO_x/CeO_2(P). The NH_3-SCR reaction over VO_x/CeO_2(P) and VO_x/CeO_2(S) catalysts mainly followed the Eley–Rideal mechanism, in which gaseous NO reacted with adsorbed NH_3 species to finally form N_2 and H_2O.

Acknowledgements

This work was financially supported by the National Natural Science Foundation of China (51108446) and the Ministry of Science and Technology of China (2012AA062506, 2013AA065301).

Notes and references

1 G. S. Qi, R. T. Yang and R. Chang, *Appl. Catal., B*, 2004, **51**, 93–106.
2 H. Bosch and F. Janssen, *Catal. Today*, 1988, **2**, 369–379.
3 Z. G. Huang, Z. P. Zhu, Z. Y. Liu and Q. Y. Liu, *J. Catal.*, 2003, **214**, 213–219.
4 G. Busca, L. Lietti, G. Ramis and F. Berti, *Appl. Catal., B*, 1998, **18**, 1–36.
5 G. Busca, M. A. Larrubia, L. Arrighi and G. Ramis, *Catal. Today*, 2005, **107–108**, 139–148.
6 J. P. Dunn, P. R. Koppula, H. G. Stenger and I. E. Wachs, *Appl. Catal., B*, 1998, **19**, 103–117.
7 P. Balle, B. Geiger and S. Kureti, *Appl. Catal., B*, 2009, **85**, 109–119.
8 I. E. Wachs and B. M. Weckhuysen, *Appl. Catal., A*, 1997, **157**, 67–90.
9 D. A. Bulushev, F. Rainone, L. Kiwi-Minsker and A. Renken, *Langmuir*, 2001, **17**, 5276–5282.
10 Z. Huang, X. Gu, W. Wen, P. Hu, M. Makkee, H. Lin, F. Kapteijn and X. Tang, *Angew. Chem., Int. Ed.*, 2012, **51**, 1–6.
11 M. Stanciulescu, G. Caravaggio, A. Dobri, J. Moir, R. Burich, J. P. Charland and P. Bulsink, *Appl. Catal., B*, 2012, **123–124**, 229–240.
12 R. Q. Long, R. T. Yang and R. Chang, *Chem. Commun.*, 2002, 452–453.
13 A. Sultana, M. Sasaki and H. Hamada, *Catal. Today*, 2011, **185**, 184–289.

14 Z. Lian, F. Liu, H. He, X. Shi, J. Mo and Z. Wu, *Chem. Eng. J.*, 2014, **250**, 390–398.
15 B. Q. Jiang, Y. Liu and Z. B. Wu, *J. Hazard. Mater.*, 2009, **162**, 1249–1254.
16 Q. Li, H. S. Yang, A. M. Nie, X. Y. Fan and X. B. Zhang, *Catal. Lett.*, 2011, **141**, 1237–1242.
17 W. Cha, S. Chin, E. Park, S.-T. Yun and J. Jurng, *Appl. Catal., B*, 2013, **140–141**, 708–715.
18 Z. P. Zhu, Z. Y. Liu, S. J. Liu and H. X. Niu, *Appl. Catal., B*, 1999, **23**, L229–L233.
19 Z. P. Zhu, Z. Y. Liu, S. J. Liu and H. X. Niu, *Appl. Catal., B*, 2001, **30**, 267–276.
20 W. Zhao, Q. Zhong, Y. X. Pan and R. Zhang, *Chem. Eng. J.*, 2013, **228**, 815–823.
21 W. Xu, Y. Yu, C. Zhang and H. He, *Catal. Commun.*, 2008, **9**, 1453–1457.
22 W. Shan, F. Liu, H. He, X. Shi and C. Zhang, *Catal. Today*, 2012, **184**, 160–165.
23 X. Gu, J. Ge, H. Zhang, A. Auroux and J. Shen, *Thermochim. Acta*, 2006, **451**, 84–93.
24 C. Li, Q. Li, P. Lu, H. Cui and G. Zeng, *Front. Environ. Sci. Eng.*, 2012, **6**, 156–161.
25 Y. Peng, C. Wang and J. Li, *Appl. Catal., B*, 2014, **144**, 538–546.
26 J. Twu, C. J. Chuang, K. I. Chang, C. H. Yang and K. H. Chen, *Appl. Catal., B*, 1997, **12**, 309–324.
27 Q. Li, X. X. Hou, H. S. Yang, Z. X. Ma, J. W. Zheng, F. Liu, X. B. Zhang and Z. Y. Yuan, *J. Mol. Catal. A: Chem.*, 2012, **356**, 121–127.
28 Y. Peng, J. Li, L. Chen, J. Chen, J. Han, H. Zhang and W. Han, *Environ. Sci. Technol.*, 2012, **46**, 2864–2869.
29 M. A. Reiche and A. Baiker, *Appl. Catal., B*, 1999, **23**, 187–203.
30 L. Chen, J. H. Li and M. F. Ge, *J. Phys. Chem. C*, 2009, **113**, 21177–21184.
31 S. Cai, D. Zhang, L. Zhang, L. Huang, H. Li, R. Gao, L. Shi and J. Zhang, *Catal. Sci. Technol.*, 2014, **4**, 93–101.
32 R. Gao, D. Zhang, X. Liu, L. Shi, P. Maitarad, H. Li, J. Zhang and W. Cao, *Catal. Sci. Technol.*, 2013, **3**, 191–199.
33 L. Zhang, J. Pierce, V. Leung, D. Wang and W. S. Epling, *J. Phys. Chem. C*, 2013, **117**, 8282–8289.
34 K. I. Hadjiivanov, *Catal. Rev.: Sci. Eng.*, 2000, **42**, 71–144.
35 C. Liu, L. Chen, J. Li, L. Ma, H. Arandiyan, Y. Du, J. Xu and J. Hao, *Environ. Sci. Technol.*, 2012, **46**, 6182–6189.
36 Z. Si, D. Weng, X. Wu, Z. Ma, J. Ma and R. Ran, *Catal. Today*, 2013, **201**, 122–130.
37 P. Forzatti, *Appl. Catal., A*, 2001, **222**, 221–236.
38 F. D. Liu, W. P. Shan, X. Y. Shi and H. Hong, *Prog. Chem.*, 2012, **24**, 445–455.
39 W. S. Kijlstra, D. S. Brands, H. I. Smit, E. K. Poels and A. Bliek, *J. Catal.*, 1997, **171**, 219–230.

